Characterization of HcaA, a novel autotransporter protein in *Helicobacter cinaedi*, and its role in host cell adhesion

Sae Aoki[a] Shigetarou Mori,[a] Hidenori Matsui,[a] Keigo Shibayama,[b] Tsuyoshi Kenri,[a] and Emiko Rimbara[a#]

[a]Department of Bacteriology II, National Institute of Infectious Diseases, Tokyo, Japan

[b]Department of Bacteriology, Nagoya University Graduate School of Medicine, Nagoya, Aichi, Japan

Running head: *Helicobacter cinaedi* autotransporter HcaA

[#]Address correspondence to Emiko Rimbara, rimbara@niid.go.jp

ABSTRACT

Helicobacter cinaedi infects the human gut and causes invasive infections such as bacteremia and cellulitis through bacterial translocation. However, the mechanism by which *H. cinaedi* attaches to host cells and establishes infection remains unclear. This study aimed to investigate the relationship between a novel putative autotransporter protein, *H. cinaedi* autotransporter protein A (HcaA), and its role in pathogenicity. The cytotoxicity of *H. cinaedi* infection in colon epithelial cell lines (Caco-2 and HT-29) was assessed using a lactate dehydrogenase assay, and it was found that cytotoxicity significantly decreased by HcaA knockout. Adhesion assays further revealed that the HcaA-knockout strain showed significantly reduced attachment to the human epithelial colorectal adenocarcinoma cell line (Caco-2) compared to that of the wild-type strain. Moreover, the recombinant HcaA protein demonstrated strong adhesion properties to the human monocytic cell line (U937). The adhesive activity was diminished when the RGD motif in HcaA was replaced with RAD, indicating that the RGD motif in HcaA is crucial for host cell adhesion. To determine the role of HcaA in *H. cinaedi* infection *in vivo*, C57BL/6 mice were orally infected with wild-type and HcaA-knockout *H. cinaedi* strains. Bacterial colonization was assesed 7, 14, and 28 days post-infection. At 7 days post-infection, colonization was significantly lower in mice infected with the HcaA-knockout strain compared to those infected with the wild-type strain. In conclusion, our findings suggest that HcaA, a novel putative autotransporter protein in *H. cinaedi*, plays a significant role as an adhesin in establishing colonization.

IMPORTANCE

Helicobacter species are classified as gastric or enterohepatic according to their habitat. Among enterohepatic *Helicobacter* species, which inhabit the intestine, colon and liver, *H. cinaedi* has been most frequently isolated from humans. *H. cinaedi* often causes bacteremia and cellulitis in immunocompromised hosts. Here, we focused on the *H. cinaedi* autotransporter protein A (HcaA), a novel virulence factor in *H. cinaedi*. We discovered that HcaA contributes to cell adhesion via its RGD motif. Furthermore, in animal experiments, bacterial colonization was reduced in mice infected with HcaA-knockout strains, supporting the hypothesis that HcaA contributes to *H. cinaedi* adhesion to host cells. Our study provides a novel mechanism for the establishment of *H. cinaedi* infections and provides new insights into the role of autotransporter proteins in the establishment of *Helicobacter* infection.

INTRODUCTION

Helicobacter species are gram-negative, helical bacilli isolated from humans and mammals. They are classified into gastric or enterohepatic *Helicobacter* species based on their habitat. *Helicobacter pylori*, a typical gastric *Helicobacter* species, infects the human stomach and is a major cause of gastric cancer (1). *H. cinaedi* is the most frequently isolated enterohepatic *Helicobacter* species strain from humans, mainly found in immunocompromised patients with bacteremia. *H. cinaedi* is responsible for recurrent cellulitis, infected aortic aneurysm, subdural hematoma, and hepatic cyst infection (2–6). *H. cinaedi* was first isolated in 1984 from a homosexual man with intestinal symptoms in Seattle and it was first isolated in Japan in 2003 (7, 8). Through *H. cinaedi* infections are predominantly reported in Japan, there have been some case reports from Denmark (9, 10). A retrospective study at a single hospital in Japan indicated that, 2.2 % of all blood culture-positive samples turned out to be *H. cinaedi*-positive when the

59 blood culture period was extended, suggesting that *H. cinaedi* infections might be overlooked
60 in other countries (11).
61 Cytolethal distending toxin (CDT) is a virulence factor in variety of gram-negative
62 pathogenic bacteria, including *H. cinaedi*. It consists of three polypeptide subunits, CdtA, CdtB,
63 and CdtC (12–14). CdtB possesses nuclease activity and causes DNA damage, leading to
64 senescence and apoptosis in host cells. CdtA and CdtC play a role in delivering CdtB into host
65 cells. Additionally, another virulence factor, *H. cinaedi* antigen CAIP (15), causes the
66 differentiation and maintenance of the pro-inflammatory profile of human macrophages and
67 triggers foam cell formation. Consequently, inflammation in atherosclerosis is induced. Studies
68 have been conducted on *H. cinaedi* biology and host-host interactions protection against
69 oxidative stress and changes in virulence via the production of alkyl hydroperoxide reductase
70 (16) as well as changes in oxygen demand during infection (17). However, the mechanisms by
71 which *H. cinaedi* interacts with host cells and establishes infection have not been fully
72 elucidated.
73 Autotransporter proteins (ATs) are type V secretion systems (T5SSs) comprising an essential
74 passenger domain that functions as the secreted portion, and an autotransporter domain with a
75 β-barrel that exports the passenger domain from the periplasm to the extracellular environment.
76 ATs are widely found in gram-negative bacteria and have diverse functions, acting as toxins
77 and adhesion factors (18). The *H. cinaedi* genome encodes a previously uncharacterized
78 putative autotransporter protein. In this study, we named this uncharacterized protein *H. cinaedi*
79 autotransporter protein A (HcaA) and investigated its contribution to *H. cinaedi* pathogenicity.
80
81 **RESULTS**
82 **Structure and localization of HcaA**

83 HcaA of *H. cinaedi* MRY 08-1234 [1,835 amino acids (aa), 197 kDa] is predicted to be
84 composed of a signal peptide (1-27 aa), passenger domain (27-1425 aa), and β-barrel domain
85 (1426-1825 aa, Fig. 1A). The β-barrel structure, characteristic of ATs, was highly supported
86 based on the pLDDT score, indicating the high confidence of the model (Fig. 1A). Therefore,
87 HcaA is predicted ATs. We constructed knockout mutants (Fig. 1B, top and middle) to identify
88 the function of HcaA. *H. cinaedi* MRY08-1234 and MRY12-0027 strains were used as host
89 strains, and *hcaA* was knocked out by replacing *hcaA* with *aphA* by homologous recombination
90 (Fig. 1B, bottom). The knockout of *hcaA* was verified by polymerase chain reaction (PCR)
91 amplification and immunoblotting using an anti-HcaA antibody (Fig. 1C and D). Immunoblot
92 analysis revealed that HcaA was localized in the membrane fraction and was not secreted (Fig.
93 1D). Fluorescence immunostaining further confirmed the presence of HcaA on the bacterial
94 surface (Fig. S1). No growth defects by the knockout of *hcaA* were observed (Fig. S2).
95
96 **HcaA knockout reduced cytotoxicity and adherence of human colon epithelial cells *in vitro***
97 The effects of the HcaA knockout on cellular cytotoxicity were evaluated *in vitro* using a
98 lactate dehydrogenase (LDH) assay. The human epithelial colorectal adenocarcinoma (Caco-2)
99 cell line and human colon cancer (HT29) cell line were infected with *H. cinaedi* MRY08-1234
100 and MRY12-0027 strains. LDH production was significantly lower in cells infected with the
101 HcaA-knockout strain than in those with the wild-type strain (Fig. 2A). Therefore, HcaA may
102 contribute to the cytotoxic effects of *H. cinaedi* infection on epithelial cells. HcaA knockout
103 did not affect LDH production by mucus-secreting HT29-MTX cells (Fig. 2A), suggesting that
104 the protective role of mucin in reducing the cytotoxicity of *H. cinaedi* was not affected by the
105 knockout of HcaA. To investigate whether CDT is involved in the reduction of cytotoxicity, we
106 analyzed its expression and observed no difference between the wild-type and HcaA-knockout
107 strains (Figure S3).

108 To determine whether HcaA contributes to cell adhesion and invasion, we performed a
109 gentamicin protection assay, and compared the rate of adherent and invaded *H. cinaedi* cells
110 between the wild-type and knockout strains. The adhesion rate of *H cinaedi* MRY08-1234 to
111 Caco-2 cells decreased significantly by HcaA knockout (Fig. 2B, upper panel). A significant
112 reduction in the adhesion rate was also observed when *H. cinaedi* MRY12-0027 was used for
113 gene knockout (Fig. 2B, bottom panel). The invasion rates of MRY08-1234 and MRY12-0027
114 were also reduced by HcaA knockout; however, the differences were not significant (Fig. 2C).
115 The invasion rate of adherent bacteria was higher in the HcaA-knockout strain (Fig. 2D).
116
117 **Adhesion was reduced in the recombinant mutant HcaA protein**
118 HcaA contains an Arg-Gly-Asp (RGD) motif at amino acid residues 348-350. To determine
119 the contribution of the RGD motif to adhesion, recombinant passenger regions of HcaA (27-
120 1,425/1,835 aa) of MRY08-1234 (WT HcaA) and mutant HcaA (with RGD motif replaced by
121 RAD) were generated (Fig. 3A). Mutant HcaA showed a significant reduction in binding to
122 U937 cells compared to that of WT HcaA ($P < 0.05$), indicating that the RGD motif contributes
123 to binding to host cells (Fig. 3B). The predicted protein structure of HcaA of MRY08-1234
124 determined using AlphaFold2 indicated that the RGD motif is located on the surface of the
125 protein, supporting the contribution of this motif to the adherence function of HcaA in *H.*
126 *cinaedi* (Fig. 3C, left). The RGD motif was conserved in all *H. cinaedi* strains registered at the
127 National Center for Biotechnology Information (NCBI), including clinical isolates (Fig. S4).
128 HcaA homologs have been reported in *H. bilis*, *H. fennelliae*, *H. canicola*, and *H. canis*, all of
129 which are closely related to *H. cinaedi* (19–21). The structural predictions for HcaA homologs
130 determined using AlphaFold2 suggest that HcaA and its homologs have structural similarities
131 in the passenger region; however, the RGD motif was present only in HcaA (Fig. 3C and D).

132 In addition, the HcaA homologs had a structure protruding from the surface, similar to the RGD
133 motif of HcaA. However, the protruding structure did not contain the RGD motif (Fig. 3C).
134
135 **Effects of HcaA on the establishment of *H. cinaedi* colonization in mice**
136 To clarify the role of HcaA in *H. cinaedi* infection *in vivo*, C57BL/6 female mice were orally
137 infected with wild-type and HcaA-knockout *H. cinaedi* strains. The recovery of *H. cinaedi* from
138 the colon, cecum, cecal contents, biceps femoris muscle, and trapezius muscle was analyzed at
139 7, 14, and 28 days post-infection (dpi). Because *H. cinaedi* is known to cause cellulitis and
140 infected aortic aneurysm (22), muscle samples were also collected in addition to the intestinal
141 tract samples. Animal experiments were performed twice, yielding consistent results. Results
142 of the first experiment, including only the MRY08-1234 strain, are shown in Fig. S5. The results
143 of the second experiment, including both MRY08-1234 and MRY12-0027 strains, are shown
144 in Figs. 4 and S6. To confirm colonization, *H. cinaedi* antibody titers in mouse serum were
145 measured. An increase in antibody titers against whole cells of *H. cinaedi* was observed in both
146 groups of infected mice. The *H. cinaedi* antibody titers tended to be higher in the group of mice
147 infected with the wild-type strain than in the mice infected with the knockout strain (Fig. 4A).
148 In the MRY08-1234 strain, the reactivity at 14 dpi was significantly higher than that in the
149 knockout strain ($P < 0.01$). Using the culture method, *H. cinaedi* was recovered from tissues
150 other than cecal contents in both groups of mice infected with the wild-type and HcaA-knockout
151 strains (Table 1). The amount of *H. cinaedi* was highest in the cecum from mice infected with
152 the wild-type strains (MRY08-1234 WT and MRY12-0027 WT) at 7 dpi (5.4×10^5 and $5.5 \times$
153 10^5 CFU/mL, respectively). The recovery rate of *H. cinaedi* from the cecum was lower in mice
154 infected with the HcaA-knockout strain (0%) than in mice infected with the wild-type strain
155 (MRY08-1234 WT, 2/6, 33.3%; MRY12-0027 WT, 2/5, 40.0%, $P = 0.12$). At 14 dpi, there
156 were fewer bacterial cells in the cecum of mice infected with the HcaA-knockout strain

157 (MRY12-0027 KO, 0/5, 0%; MRY08-1234 KO, 1/5, 20%) strain than in mice infected with the
158 wild-type strain (MRY12-0027, 2/5, 40.0%; MRY08-1234, 4/5, 80.0%, $P = 0.06$). In MRY08-
159 1234, there was a trend towards a lower number of bacterial cells in the colon of mice infected
160 with the HcaA-knockout strain than with the wild-type strain at 14 dpi. Similarly, in MRY12-
161 0027, there were also fewer bacterial cells in mice infected with the HcaA-knockout strain
162 (MRY12-0027 ΔHcaA, 0/5, 0%) than in mice infected with the wild-type strain (MRY12-0027
163 WT, 5/5, 100%). For the cecum and colon, in which bacteria were frequently detected by the
164 culture method, mRNA was extracted and bacteria were detected by quantitative real-time PCR
165 (qPCR). The frequency of positive samples was higher in the group of mice infected with the
166 wild-type strain than in mice infected with the knockout strain (Fig. S6). Therefore, a combined
167 analysis of the results of the culture and qPCR assays showed that the frequency of positive
168 detection was higher for mice infected with the wild-type strain than in mice infected with the
169 HcaA-knockout (Fig. 4B). A reduction in the number of HcaA-knockout bacterial cells was
170 also observed by an immunofluorescence analysis of the colon infected with *H. cinaedi* using
171 an anti-*H. cinaedi* antibody (Figs. 4C and S5). *H. cinaedi* was observed in the mucosal
172 epithelium, regardless of the presence or absence of HcaA and the duration of infection;
173 however, the number of bacteria tended to be lower in samples from mice infected with the
174 HcaA-knockout strain than in samples from mice infected with the wild-type strain.
175

176 **DISCUSSION**

177 Enterohepatic *Helicobacter* species are increasingly recognized as critical pathogens in
178 mammals. Among them, *H. cinaedi* causes bacteremia, cellulitis, and infected aortic aneurysms
179 in humans (2, 4, 23). Although *H. cinaedi* infections are rarely reported, cases have been
180 increasing in Japan since 2003 (8, 11, 23). However, little is known about the virulence factors
181 of *H. cinaedi*. ATs have various functions that contribute to the establishment of infections by

182 pathogenic gram-negative bacteria. In this study, we found that HcaA, an ATs, is responsible
183 for adhesion to host cells and contributes to the pathogenesis of *H. cinaedi* infection. This is the
184 first report to elucidate the role of ATs in enterohepatic *Helicobacter* species.

185 T5SS proteins are classified into subgroups labelled Va–Ve; however, this classification is
186 based on protein architecture and does not reflect the functions of the secreted passengers. VacA
187 produced by *H. pylori* is classified as a type Va AT; it binds to host cells and is internalized,
188 causing vacuolation characterized by the accumulation of large vesicles (24). Serine protease
189 autotransporters of *Enterobacteriaceae* (SPATEs) produced by *Enterobacteriaceae* are also
190 classified as type Va ATs (25). SPATEs exhibit protease activity to cleave host proteins. HcaA
191 is structurally similar to EspP, SPATEs in *Escherichia coli*. We did not detect protease activity
192 against casein and pepsin, the major substrates for SPATEs (Fig. S7a and b). Furthermore, no
193 significant differences in CDT expression were observed in the presence or absence of HcaA
194 (Fig. S3). In contrast, the number of bacterial cells adhering to human epithelial cells and the
195 level of cytotoxicity were significantly reduced by HcaA knockout. These findings suggest that
196 the reduced cytotoxicity observed in the HcaA-knockout strain can be explained by the decrease
197 in the number of adherent *H. cinaedi* cells, rather than a direct cytotoxic effect of HcaA itself.

198 HcaA contains the RGD motif in its passenger region. The RGD motif acts as a fibronectin
199 cell adhesion site. It plays a role in adhesion to host epithelial cells that express receptors of the
200 RGD motif, such as integrins (26). Cell adhesion experiments using purified WT HcaA with
201 the RGD motif and mutant HcaA with the RAD motif showed that the adhesion ability
202 decreased significantly when RGD was replaced by RAD. Structural prediction indicated that
203 the RGD motif is located on the surface of HcaA at an externally protruding site. The RGD
204 motif is known to bind to integrins, which are thought to mediate the adhesion of HcaA to cells.
205 Our results strongly suggest that the RGD motif of HcaA plays a role in cell adhesion. However,
206 the adhesion ability of HcaA was not completely diminished by replacing RGD with RAD.

207 Therefore, HcaA may function as an adhesin independent of the RGD motif, and the presence
208 of the RGD motif enhances its ability to adhere to cells. HcaA homologs in other enterohepatic
209 *Helicobacter* species, such as *H. bilis*, *H. canis*, *H. fennelliae,* and *H. canicola,* lacked the RGD
210 motif (Fig. 3). In addition, the RGD motif of HcaA was highly conserved among *H. cinaedi*
211 strains, regardless of strain origin (Fig. S4). *H. canicola* is genetically most closely related to
212 *H. cinaedi* (21). However, a phylogenetic analysis indicated that HcaA is most similar to the
213 HcaA homolog of *H. fennelliae* and not to that of *H. canicola*. *H. fennelliae* is the second most
214 common enterohepatic *Helicobacter* species causing invasive infections in humans. The
215 structural similarity between HcaA and HcaA homologs of *H. fennelliae* suggests that HcaA
216 plays a critical role in the pathogenesis of enterohepatic *Helicobacter* species in humans. The
217 results of comparative genomic analyses indicate that *H. cinaedi* is a human-adapted lineage,
218 unlike *H. canicola* (21). The acquisition of the RGD motif of HcaA during the evolution of *H.*
219 *cinaedi* may have contributed to the adaptation of *H. cinaedi* to humans, resulting in a higher
220 isolation rate of *H. cinaedi* from humans compared to other enterohepatic *Helicobacter* species.
221 Further investigation is needed to identify the HcaA-binding target in the host cell.
222 The mouse infection experiment also supported the results of *in vitro* analyses, showing that
223 HcaA knockout reduced the number of infected bacterial cells in the cecum and colon of *H.*
224 *cinaedi*-infected mice. In particular, the HcaA-knockout strain had significantly fewer bacterial
225 cells in culture than that in the wild-type strain at 7 dpi. Therefore, HcaA plays an important
226 role in the established phase of *H. cinaedi* infection. A similar effect was observed for FaaA
227 (flagella-associated autotransporter A), an AT possessed by *H. pylori* contributing to gastric
228 colonization, and an FaaA deficiency has been reported to significantly reduce the number of
229 colonized bacteria in the early stages of infection (27).
230 ATs have various functions. For example, ImaA, another ATs in *H. pylori,* is essential for
231 host colonization and modulates the host inflammatory response via the inflammatory cytokines

232 IL-8 and TNF-α (28). In addition, EspC, SPATEs, degrades various host proteins, such as
233 hemoglobin and mucin, and also to prevent cytotoxicity during the initial stage of bacterial
234 infection by regulating pore formation (25, 29). Thus, similar to other ATs, HcaA can also have
235 multiple functions related to the establishment of chronic *H. cinaedi* infections in humans.
236 Further analyses are needed to elucidate additional functions of HcaA beyond its role in cell
237 adhesion.

238 This study identified a novel virulence factor of *H. cinaedi*, HcaA, as an adhesin protein.
239 HcaA was shown to play an essential role in the establishing *H. cinaedi* infection both *in vitro*
240 and *in vivo*. On the other hand, adhesion was also observed in the HcaA-knockout strain,
241 although it was reduced compared to that of the wild-type strain, suggesting that factors other
242 than HcaA contribute to host adhesion. Further studies of HcaA and other factors are needed to
243 understand the interaction between *H. cinaedi* and host cells.

244

245 **MATERIALS AND METHODS**

246 **Condition of bacterial strains and host cells**

247 *H. cinaedi* strains MRY08-1234 (MLST: ST10) and MRY12-0027 (MLST: ST15) isolated
248 from the blood of patients with bacteremia in Japan were used throughout the study. The *H.*
249 *cinaedi* strains were cultured as described previously (30). Briefly, strains were subcultured on
250 Brucella agar (Becton, Dickinson, Franklin Lakes, NJ, USA) with 5% horse blood at 37 °C
251 under microaerobic conditions with hydrogen generated by the gas exchange method using an
252 anaerobic gas mixture (H_2, 10%; CO_2, 10%; and N_2, 80%). For liquid culture, bacteria were
253 suspended in Brucella broth (Becton, Dickinson) with 10% fetal bovine serum (FBS;
254 NICHIREI), and the culture was incubated at 37 °C under microaerobic conditions with
255 hydrogen.

256 Human epithelial colorectal adenocarcinoma cells (Caco-2), a human myelomonocyte cell

257 line (U937), a human colon cancer cell line (HT29), and mucus-secreting HT29 cells (HT29-
258 MX) were used in this study. Caco-2 cells were maintained in Eagle's minimum essential
259 medium (EMEM, Sigma Aldrich, St. Louis, MO, USA) containing 2 mM L-glutamine, 1 mM
260 sodium pyruvate, 1.5 mg/L sodium bicarbonate, 10 mg/L phenol red, 10% heat-inactivated
261 (56 °C, 30 min) FBS, 1% non-essential amino acids. U937, HT29, and HT29-MX cells were
262 maintained in RPMI 1640 (Sigma Aldrich) with 10% heat-inactivated FBS. All media
263 contained an antimicrobial cocktail (penicillin-streptomycin), except for the *H. cinaedi*
264 infection experiments. All cells were incubated in a 5% CO_2, humidified atmosphere at 37 °C,
265 in a stationary manner.
266
267 **Generation of *hcaA* deletion mutants and antibodies to HcaA**
268 Knockout mutants were generated according to previously described methods (30). Briefly,
269 1,000 base pairs up- and downstream of *hcaA* were PCR-amplified. The primers contained a
270 linker sequence overlapping with *aphA*. To obtain the construct of *aphA* sandwiched by the
271 target gene sequence, three purified PCR products, up- and downstream of *hcaA* and *aphA*,
272 were mixed and amplified. The donor fragment was electroporated into *H. cinaedi*. The
273 transformed *H. cinaedi* was plated on agar plates containing 10 μg/mL kanamycin and 3% agar.
274 After incubation, the growing colonies were selected as knockout mutants. The knockout of
275 *hcaA* was confirmed by PCR and an immunoblot analysis. Primers used for cloning and PCR
276 are listed in Table S1. For the immunoblot analysis, the whole bacterial cell lysates, culture
277 supernatant, soluble fraction, and membrane fraction were prepared as follows. The bacterial
278 culture was incubated until an optical density at 600 nm (OD600) of 0.4, and the supernatant
279 was collected by centrifugation (8,600 ×*g*, 10 min, 4 °C). Then, the insoluble and the soluble
280 fractions were prepared by extracting proteins from the pellet using the EzBactYeast Crusher
281 (ATTO Corp., Tokyo, Japan) and by centrifugation. The insoluble fraction was used as the

282 membrane fraction. These samples were separated and transferred to Immobilon™ -FL PVDF
283 (pore size, 0.45 um; Millipore Inc., Burlington, MA, USA) using a semidry electroblotting
284 system. An anti-HcaA antibody was obtained by immunizing rabbits with a KLH-conjugated
285 peptide (RGDMPQESKTLEQN corresponding to positions 348–361 of HcaA in MRY08-
286 1234), followed by affinity purification against the peptide. The resulting rabbit polyclonal
287 HcaA antibody was used as the primary antibody for the immunoblot analysis (1:1,000), and
288 peroxidase-conjugative AffiniPure donkey anti-mouse IgG (H+L) (Jackson ImmunoResearch
289 Inc., 1:50,000) was used as the secondary antibody. The bands were visualized using ECL
290 Select (Amersham Biosciences, Amersham, UK) and Amersham™ ImageQuant 800
291 (Amersham Biosciences).
292
293 **Cell infection experiments**
294 Strains were grown in Brucella broth with 10% FBS at 37 °C under microaerobic conditions.
295 After incubation, the bacterial culture was inoculated into 10 mL of fresh broth, and the culture
296 was incubated until an OD600 of 0.4. Bacterial cells were harvested by centrifugation (3,350 ×
297 *g*, 10 min, 25 °C) and resuspended in the appropriate medium for each cell. Infections were
298 performed at a multiplicity of infection (MOI) of 100. Immediately after the addition of bacteria,
299 the plates were centrifuged at 300 ×*g* for 5 min at 25 °C, followed by incubation in 5% CO_2
300 humidified atmosphere, at 37 °C for 4 h.
301 Cytotoxicity was evaluated by measuring lactate dehydrogenase using the Cytotoxicity LDH
302 Assay Kit-WST (Dojindo Laboratories, Tokyo, Japan). The assay was performed according to
303 the manufacturer's instructions.
304 Cell adhesion and invasion ability were evaluated using a gentamicin assay. To evaluate
305 adhesion ability, cells were liberated by trypsinization, seeded into a 24-well tissue culture-
306 treated polystyrene flat-bottom microtiter plate (FALCON), and incubated to confluence. Caco-

307 2 cells were infected by adding 1 mL of bacterial suspension (MOI 100) directly to each well.
308 After 4 h of incubation, the un-bound bacteria were removed by washing with pre-warmed PBS.
309 To evaluate invasive ability, *H. cinaedi* adherent to Caco-2 cells was incubated in EMEM with
310 gentamicin at 250 μg/mL. After 1.5 h, the infected cells were washed with pre-warmed PBS.
311 For both assays, host cells were washed with PBS containing 0.1% saponin (FUJIFILM Wako
312 Pure Chemical Co., Osaka, Japan). Serial dilutions of the suspension were plated on Brucella
313 agar containing 5% horse blood and 3% agar. After incubation, colonies were counted, and the
314 adhesion rate (%), invasion rate (%), and the invasion rate of adherent bacteria (%) were
315 calculated.
316
317 **Purification of HcaA**
318 To produce recombinant HcaA, we constructed expression vectors; *hcaA* was amplified by
319 PCR and introduced into pCold™ I DNA (TaKaRa, Shiga, Japan) using the In-Fusion® HD
320 Cloning Kit. gDNA from *H. cinaedi* strain MRY08-1234 was used to amplify the passenger
321 region of HcaA (27-1,425/1,835 aa). The expression vector containing the passenger region of
322 HcaA was transferred into *Escherichia coli* BL21 (DE3) pLysS cells and plated on LB agar
323 plates containing 100 μg/mL ampicillin. The growing colonies were inoculated into 100 mL of
324 LB broth containing 100 μg/mL ampicillin and incubated at 37 °C with shaking at 200 rpm for
325 3 h. The cells were then transferred to 900 mL of fresh medium and grown in a 2 L flask at
326 37 °C until OD600 of 0.6. Protein expression was induced by cooling in ice water for 1 h and
327 adding 400 μL of 1 mM isopropyl β-D-thiogalactopyranoside. Recombinant HcaA was
328 expressed as a fusion protein containing a histidine tag. The cell cultures were further incubated
329 at 15 °C overnight. Bacteria were harvested by centrifugation at 5,000 ×*g* for 10 min at 4 °C
330 and resuspended in 20 mM Tris-HCl (Nacalai, Kyoto, Japan), 150 mM NaCl (FUJIFILM
331 Wako), and 40 mM imidazole (FUJIFILM Wako) at pH 7.6 with cOmplete™ Protease Inhibitor

332 Cocktail (Roche Molecular Systems). The suspended solution was sonicated on ice, and the
333 supernatant was collected by centrifugation at 5,000 ×*g* for 45 min at 4 °C. The recombinant
334 protein was purified in two steps using an affinity column (HisTrap FF crude, Cytiva), followed
335 by size exclusion chromatography (Superdex™ 200 Increase 10/300 GL, Cytiva). To replace
336 the RGD motif of the HcaA protein with RAD, site-directed mutagenesis of the HcaA
337 expression vector was performed using PrimeSTAR® GXL DNA Polymerase. The primers
338 used to generate expression vectors are listed in Table S1.
339
340 **Adhesion assay of HcaA to U937 cells**
341 Purified HcaA and mutant HcaA were prepared at a concentration of 50 μg/mL in PBS,
342 dispensed in 100 μL aliquots to 96-well plates, and fixed to the bottom of the plates by
343 incubation overnight at 4 °C. The wells were then washed with PBS and blocked by adding 2%
344 BSA in PBS and incubated again overnight at 4 °C. U937 cells were incubated until confluence
345 and then diluted with MEM to a concentration of 1×10^5 cells/mL. The use of U937 cells in
346 this assay was based on previous analyses of their activity in relation to *H. pylori* (31).
347 Fluorescein (FUJIFILM Wako) was added to the cell suspension at a final concentration of 1
348 mg/mL and incubated at 37 °C for 30 min. After washing, MEM containing 2 mM Ca and 2
349 mM Mg was added and allowed to react for 30 min on ice in the dark. The cell suspension,
350 diluted to a concentration of 5×10^5 /mL, was then added to HcaA-coated plates and incubated
351 at 37 °C for 1 h. After washing and replacement with phenol red-free MEM medium (Sigma),
352 fluorescence was measured, and the number of cells bound to purified proteins was observed.
353
354 **Sequence alignment, phylogenetic analysis, and structure prediction of HcaA and HcaA**
355 **homologs**
356 Amino acid sequences of HcaA homologs in other enterohepatic *Helicobacter* species were

357 obtained from the whole genome sequences of *H. bilis* ATCC43879 (Accession No. KI392040),
358 and *H. fennelliae* MRY12-0050 (Accession No. BSAD00000000), and *H. canicola* PAGU1409
359 (Accession no. DRR092854) and *H. canis* CCUG32756 (Accession No. GCF008693005) were
360 obtained from the National Center for Biotechnology Information (NCBI). The passenger
361 regions of the amino acid sequences of the HcaA and HcaA homologs were aligned using
362 ClustalW ver. 2.1 (32), and visualized using CLC Genomics Workbench Version 22.0.1
363 (QIAGEN). A phylogenetic tree based on the aligned amino acid sequences of the passenger
364 domain of HcaA and HcaA homologs was constructed using RAxML-NG v1.1.0
365 (https://github.com/amkozlov/raxml-ng) and visualized using MEGA X v 10.2.6 (33).
366 The prediction of the structures of HcaA and HcaA homologs were performed using
367 AlphaFold2 Ver.2.2.2 on the supercomputer system of the Institute for Chemical Research,
368 Kyoto University, with a full dBs preset.
369
370 **Animal experiments and infection**
371 Animal experiments were performed twice; the results of the first animal experiment are
372 shown in the Supplementary Appendix, and the results of the second experiment are reported
373 in the manuscript. Six-week-old female C57BL/6 mice (Japan SLC, Inc., Shizuoka, Japan)
374 maintained under specific pathogen-free conditions were used in this study. Mice were fed a
375 standard rodent chow, given ad libitum access to water, housed in microisolator cages, and
376 isolated from specific pathogens.
377 Strains were suspended in PBS at 1×10^9 cells/mL. The mice were then orally administered
378 0.2 mL of each bacterial suspension through a 1 mL syringe attached to an oral probe every
379 other day for a total of three times. The same volume of PBS was administered to mice as a
380 negative control. There were 14 mice in the control group, 15 mice in the wild-type strain
381 infection group, and 16 mice in the HcaA-knockout strain infection group.

382 On days 7, 14, and 28 after inoculation, five or six mice from each group were sacrificed for
383 analyses. The blood, cecal contents, colon, biceps femoris muscle, and trapezius muscle were
384 collected aseptically for further analysis. All animal experiments and the study protocol were
385 approved by the Committee for Animal Experimentation of the National Institute of Infectious
386 Diseases (approval number 121126).
387
388 **ELISA**
389 To measure *H. cinaedi* antibody titers in mouse serum, an enzyme-linked immunosorbent
390 assay (ELISA) was performed as described previously (34). To prepare serum, whole blood
391 collected at autopsy was incubated at 4 °C and then centrifuged at 2,000 ×*g* for 5 min at 4 °C.
392 The supernatant was collected, mixed with glycerol (50% final concentration), and designated
393 as serum. To prepare whole-cell lysates, *H. cinaedi* MRY08-1234 cells were disrupted by
394 sonication. Each well of Nunc-Immuno 96-well microtiter plates (No. 439454; Thermo Fisher
395 Scientific, Waltham, MA, USA) was coated with of whole-cell lysates (4 ug/mL in 0.1 M
396 carbonate/bicarbonate buffer, pH 9.4). After overnight incubation at 4 °C, the plate was washed
397 with PBS containing 0.05% (vol/vol) Tween 20 (PBS-T), and the wells were saturated with
398 blocking buffer (PBS containing 1% BSA) and incubated for 1 h at 37 °C while shaking at 500
399 rpm. After washing with PBS-T, the wells were filled with serum samples, which were diluted
400 100-fold with a blocking buffer. The dilution of serum was determined by preliminary
401 experiments (Fig. S8). Plates were incubated for 1 h at 37 °C with shaking at 500 rpm.
402 Horseradish peroxidase-conjugated goat anti-mouse IgG secondary antibody (Jackson, Bar
403 Harbor, ME, USA) diluted 5,000-fold in blocking buffer was used. Absorbance was measured
404 at 450 nm using a Multiskan FC microplate reader (Thermo Scientific).
405
406 **Isolation and detection of *H. cinaedi* from infected mice**

407 Culture and PCR were used to assess *H. cinaedi* infection in each organ. For the cultivation
408 of *H. cinaedi*, agar plates containing Skirrow (Oxoid), 5% horse blood, 3% agar, and 4 μg/mL
409 ciprofloxacin (FUJIFILM Wako) were inoculated with the cecal contents, colon, biceps femoris
410 muscle and trapezius muscle that had been homogenized in Brucella broth. MRY08-1234 is
411 resistant to ciprofloxacin; accordingly, ciprofloxacin was added to eliminate commensal
412 intestinal bacteria in mice and isolate only *H. cinaedi*. Plates were incubated at 37 °C under
413 microaerobic conditions. The growth of the colonies was confirmed by the detection of *cdt*
414 using PCR. We also evaluated total RNA of *H. cinaedi*. Samples were homogenized with 1 mL
415 of Isogen (Nippon Gene, Toyama, Japan). The homogenates were supplemented with 0.2 mL
416 of chloroform (Sigma Aldrich) and mixed. The samples were then centrifuged (12,000 ×*g*, 15
417 min, 4 °C), and the aqueous layer was transferred to new tubes. RNA was precipitated by
418 combining 500 μL of isopropanol with the aqueous layer, followed by incubation at room
419 temperature for 10 min and centrifugation as described above. Total RNA was extracted from
420 the supernatant using the PureLink® RNA Mini Kit (Thermo Fisher Scientific, Waltham, USA)
421 according to the manufacturer's instructions. The extracted RNA was used for quantitative real-
422 time PCR (qPCR). Reverse transcription and reverse transcription quantitative PCR (RT-qPCR)
423 were performed using ReverTra Ace qPCR RT Master Mix with gDNA Remover (Toyobo,
424 Osaka, Japan), THUNDERBIRD™ SYBR qPCR MIX (Toyobo), and Applied Biosystems®
425 7500Fast (Thermo Fisher Scientific). Primers for PCR and qPCR are listed in Table S2.
426
427 **Histology and Fluorescence imagines**
428 Colons from mice were harvested and fixed with a 4% paraformaldehyde phosphate buffer
429 solution (FUJIFILM Wako). Sections obtained from fixed specimens were permeabilized and
430 incubated with an anti-*H. cinaedi* antibody (1:1,000) as the first antibody at room temperature
431 for 1 h. The anti-*H. cinaedi* antibody was obtained by immunizing rabbits with heat-inactivated

432 *H. cinaedi* MRY08-1234 as an antigen, followed by protein A-purification. The sections were
433 then rinsed and stained with Alexa Fluor 488 (*H. cinaedi*) and 4',6-diamidino-2-phenylindole
434 (nuclei). Fluorescence signals were visualized using an automated slide scanning system
435 (Olympus VS200, Olympus, Tokyo, Japan) and images were analyzed using ImageJ ver.1.53t.
436

437 **Statistical analysis**

438 Differences in the recovery of *H. cinaedi* by culture from infected mice were analyzed using
439 Fisher's exact tests. For other experiments, the Mann–Whitney test was used for comparison.
440 All statistical analyses were performed using GraphPad Prism version 9.4.1 and differences
441 were considered statistically significant when the *P*-value was <0.05.
442

443 **ACKNOWLEDGMENTS**

444 This work was supported by JSPS KAKENHI Grant Numbers 16K18928, 19K07074 (E. R.)
445 and 22K15465 (S. A.), the GSK Japan Research Grant 2017 (E. R.) and by AMED
446 JP20fk0108148 (E. R.).
447

448 **CONFLICT OF INTEREST**

449 The authors declare no conflicts of interest.

450 **References**

451 1. Polk DB, Peek RM. 2010. *Helicobacter pylori*: Gastric cancer and beyond. 6. Nat Rev Cancer
452 10:403–414. https://doi.org/10.1038/nrc2857.

453 2. Matsuo T, Mori N, Mizuno A, Sakurai A, Kawai F, Starkey J, Ohkushi D, Abe K, Yamasaki
454 M, Ito J, Yoshino K, Mikami Y, Uehara Y, Furukawa K. 2020. Infected aortic aneurysm caused
455 by *Helicobacter cinaedi*: Case series and systematic review of the literature. BMC Infect Dis
456 20:854. https://doi.org/10.1186/s12879-020-05582-7.

457 3. Akiyama T, Imamura H, Fukui N, Sakai N. 2021. *Helicobacter cinaedi*-infected chronic
458 subdural hematoma mimicking an expanding hematoma: A case report. Surg Neurol Int 12:288.
459 https://doi.org/10.25259/SNI_387_2021.

460 4. Kawamura Y, Tomida J, Morita Y, Fujii S, Okamoto T, Akaike T. 2014. Clinical and
461 bacteriological characteristics of *Helicobacter cinaedi* infection. J Infect 0Chemother 20:517–
462 526. https://doi.org/10.1016/j.jiac.2014.06.007.

463 5. Suzuki T, Kutsuna S, Tsuboi M, Ota M, Hayakawa K, Ohmagari N. 2019. *Helicobacter*
464 *cinaedi* hepatic cyst infection with bacteremia. Emerg Infect Dis 25:603–604.
465 https://doi.org/10.3201/eid2503.180936.

466 6. Saito J, Rimbara E, Inaguma S, Hasegawa C, Kamiya S, Mizuno A, Sone Y, Ogawa T,
467 Numata Y, Takahashi S, Asano M. 2022. Determining infected aortic aneurysm treatment using
468 focused detection of *Helicobacter cinaedi*. Emerg Infect Dis 28:1494–1498.
469 https://doi.org/10.3201/eid2807.212505.

470 7. Totten PA, Fennell CL, Tenover FC, Wezenberg JM, Perine PL, Stamm WE, Holmes KK.
471 1985. *Campylobacter cinaedi* (sp. nov.) and *Campylobacter fennelliae* (sp. nov.): Two New
472 *Campylobacter* species Associated with Enteric Disease in Homosexual Men. J Infect Dis

473 151:131–139. https://doi.org/10.1093/infdis/151.1.131.

474 8. Murakami H, Iwata M, Goto M, Takahashi T, Ono E, Sawabe E, Okuzumi K, Yamaguchi K,
475 Takahashi T. 2003. Isolation of *Helicobacter cinaedi* from blood of an immunocompromised
476 patient in Japan. J Infect Chemother 9:344–347. https://doi.org/10.1007/s10156-003-0265-3.

477 9. Holst H, Andresen K, Blom J, Højlyng N, Kemp M, Krogfelt KA, Christensen JJ. 2008. A
478 case of *Helicobacter cinaedi* bacteraemia in a previously healthy person with cellulitis. Open
479 Microbiol J 2:29–31. https://doi.org/10.2174/1874285800802010029.

480 10. Nielsen HL, Prag J, Krogfelt KA. 2015. *Helicobacter cinaedi* knee infection after
481 arthroscopy in an immunocompetent patient. BMJ Case Rep 2015:bcr2014208637.
482 https://doi.org/10.1136/bcr-2014-208637.

483 11. Araoka H, Baba M, Kimura M, Abe M, Inagawa H, Yoneyama A. 2014. Clinical
484 characteristics of bacteremia caused by *Helicobacter cinaedi* and time required for blood
485 cultures to become positive. J Clin Microbiol 52:1519–1522.

486 12. Guerra L, Cortes-Bratti X, Guidi R, Frisan T. 2011. The biology of the cytolethal distending
487 toxins. Toxins 3:172–190. https://doi.org/10.3390/toxins3030172.

488 13. Taylor NS, Ge Z, Shen Z, Dewhirst FE, Fox JG. 2003. Cytolethal distending toxin : A
489 potential virulence factor for *Helicobacter cinaedi*. J Infect Dis 188:1892–1897.

490 14. Scuron MD, Boesze-Battaglia K, Dlakić M, Shenker BJ. 2016. The Cytolethal distending
491 toxin contributes to microbial virulence and disease pathogenesis by acting as a tri-perditious
492 toxin. Front Cell Infect Microbiol 6:168.

493 15. D'Elios MM, Vallese F, Capitani N, Benagiano M, Bernardini ML, Rossi M, Rossi GP,
494 Ferrari M, Baldari CT, Zanotti G, de Bernard M, Codolo G. 2017. The *Helicobacter cinaedi*

495 antigen CAIP participates in atherosclerotic inflammation by promoting the differentiation of
496 macrophages in foam cells. Sci Rep 7:40515. https://doi.org/10.1038/srep40515.

497 16. Charoenlap N, Shen Z, McBee ME, Muthupalani S, Wogan GN, Fox JG, Schauer DB. 2012.
498 Alkyl hydroperoxide reductase is required for *Helicobacter cinaedi* intestinal colonization and
499 survival under oxidative stress in BALB/c and BALB/c interleukin-10−/− mice. Infect Immun
500 80:921–928. https://doi.org/10.1128/IAI.05477-11.

501 17. Schmitz JE, Taniguchi T, Misawa N, Cover TL. 2016. Epithelial coculture and l-lactate
502 promote growth of *Helicobacter cinaedi* under H2-free aerobic conditions. Appl Environ
503 Microbiol 82:6701–6714. https://doi.org/10.1128/AEM.01943-16.

504 18. Meuskens I, Saragliadis A, Leo JC, Linke D. 2019. Type V Secretion Systems: An
505 Overview of Passenger Domain Functions. Frontiers in Microbiology 10.

506 19. Flahou B, Haesebrouck F, Smet A, Yonezawa H, Osaki T, Kamiya S. 2013. Gastric and
507 enterohepatic Non-*Helicobacter pylori* Helicobacters. Helicobacter 18 Supplement 1:66–72.
508 https://doi.org/10.1111/hel.12072.

509 20. Saito S, Tsukahara M, Ohkusu K, Kurai H. 2016. *Helicobacter fennelliae* bacteremia Three
510 Case Reports and Literature review. Med (Baltim) 95:e3556.
511 https://doi.org/10.1097/MD.0000000000003556.

512 21. Gotoh Y, Atsuta Y, Taniguchi T, Nishida R, Nakamura K, Ogura Y, Misawa N, Hayashi T
513 2022. *Helicobacter cinaedi* is a human-adapted lineage in the *Helicobacter*
514 *cinaedi/canicola/'magdeburgensis'* complex. Microbial Genomics 8.
515 https://doi.org/10.1099/mgen.0.000830.

516 22. Taniguchi T, Yamazaki W, Saeki Y, Takajo I, Okayama A, Hayashi T, Misawa N. 2016.

517 The pathogenic potential of *Helicobacter cinaedi* isolated from non-human sources: Adherence,
518 invasion and translocation ability in polarized intestinal epithelial Caco-2 cells in vitro. 4. J Vet
519 Med Sci 78:627–632. https://doi.org/10.1292/jvms.15-0595.

520 23. Matsumoto T, Goto M, Murakami H, Tanaka T, Nishiyama H, Ono E, Okada C, Sawabe E,
521 Yagoshi M, Yoneyama A, Okuzumi K, Tateda K, Misawa N, Yamaguchi K. 2007. Multicenter
522 study to evaluate bloodstream infection by *Helicobacter cinaedi* in Japan. J Clin Microbiol
523 45:2853–2857. https://doi.org/10.1128/JCM.00465-07.

524 24. Palframan SL, Kwok T, Gabriel K. 2012. Vacuolating cytotoxin A (VacA), a key toxin for
525 *Helicobacter pylori* pathogenesis. Front Cell Infect Microbiol 2:92.
526 https://doi.org/10.3389/fcimb.2012.00092.

527 25. Dautin N. 2010. Serine protease autotransporters of *Enterobacteriaceae* (SPATEs):
528 Biogenesis and Function. Toxins 2:1179–1206. https://doi.org/10.3390/toxins2061179.

529 26. D'Souza SE, Ginsberg MH, Plow EF. 1991. Arginyl-glycyl-aspartic acid (RGD): A cell
530 adhesion motif. Trends Biochem Sci 16:246–250. https://doi.org/10.1016/0968-
531 0004(91)90096-E.

532 27. Radin JN, Gaddy JA, González-Rivera C, Loh JT, Algood HMS, Cover TL. 2013. Flagellar
533 localization of a *Helicobacter pylori* autotransporter protein. mBio 4:e00613-e00612.
534 https://doi.org/10.1128/mBio.00613-12.

535 28. Sause WE, Castillo AR, Ottemann KM. 2012. The *Helicobacter pylori* autotransporter
536 ImaA (HP0289) modulates the immune response and contributes to host colonization. Infect
537 Immun 80:2286–2296. https://doi.org/10.1128/IAI.00312-12.

538 29. Guignot J, Segura A, Nhieu GTV. 2015. The serine protease EspC from enteropathogenic

539 *Escherichia coli* regulates pore formation and cytotoxicity mediated by the Type III secretion
540 system. PLOS Pathog 11:e1005013. https://doi.org/10.1371/journal.ppat.1005013.

541 30. Rimbara E, Mori S, Kim H, Suzuki M, Shibayama K. 2018. Mutations in genes encoding
542 penicillin-binding proteins and efflux pumps play a role in β-lactam resistance in *Helicobacter*
543 *cinaedi*. Antimicrob Agents Chemother 62:e02036-17. https://doi.org/10.1128/AAC.02036-17.

544 31. Shibayama K, Takeuchi H, Wachino J, Mori S, Arakawa Y. 2011. Biochemical and
545 pathophysiological characterization of *Helicobacter pylori* asparaginase. Microbiol Immunol
546 55:408–417. https://doi.org/10.1111/j.1348-0421.2011.00333.x.

547 32. Larkin MA, Blackshields G, Brown NP, Chenna R, McGettigan PA, McWilliam H,
548 Valentin F, Wallace IM, Wilm A, Lopez R, Thompson JD, Gibson TJ, Higgins DG. 2007.
549 Clustal W and Clustal X version 2.0. Bioinformatics 23:2947–2948.
550 https://doi.org/10.1093/bioinformatics/btm404.

551 33. Kumar S, Stecher G, Li M, Knyaz C, Tamura K. 2018. MEGA X: Molecular evolutionary
552 genetics analysis across computing platforms. Mol Biol Evol 35:1547–1549.
553 https://doi.org/10.1093/molbev/msy096.

554 34. Matsui H, Suzuki M, Isshiki Y, Kodama C, Eguchi M, Kikuchi Y, Motokawa K, Takaya A,
555 Tomoyasu T, Yamamoto T. 2003. Oral immunization with ATP-dependent protease-deficient
556 mutants protects mice against subsequent oral challenge with virulent *Salmonella enterica*
557 serovar Typhimurium. Infect Immun 71:30–39. https://doi.org/10.1128/IAI.71.1.30-39.2003.

558

559
560 **Table and figure legends**

Table 1. Recovery of *H. cinaedi* from tissues of *H. cinaedi*-infected mice

	Limit of detection of mice tested (CFU mL^{-1})											
	Post-infection (days)											
	MRY08-1234 WT			MRY08-1234 KO			MRY12-0027 WT			MRY12-0027 KO		
Tissue	7	14	28	7	14	28	7	14	28	7	14	28
Cecal contents	0	0	0	0	0	0	0	0	0	0	0	0
Cecum	5.5×10^5	1.5×10^3	1.5×10^3	0	0	1.5×10^3	5.4×10^5	1.2×10^3	0	0	0	1.5×10^3
Colon	1.8×10^3	2.5×10^3	4.0×10^3	0	0	6.0×10^2	1.6×10^3	2.0×10^3	9.0×10^3	0	0	6.0×10^2
Biceps femoris muscle	0	0	2.0×10^2	0	5.0×10^2	1.0×10^1	0	0	0	0	0	0
Trapezius muscle	0	5.0×10^2	0	0	0	0	0	5.0×10^2	0	0	0	0

WT, wild type; KO, HcaA-knockout

561 **Figure legends**

562 Fig. 1. Construction of *hcaA*-knockout strains.

563 (A) HcaA contains features of putative autotransporter proteins. The three-dimensional
564 structure of HcaA predicted by AlphaFold2 is color-coded by pLDDT values, which indicate
565 the confidence level of the prediction. (B) Schematic diagram of the knockout strategy for the
566 *hcaA* gene. The *hcaA* locus on *H. cinaedi* MRY12-0027 and MRY08-1234 chromosomes, the
567 donor fragment used to disrupt the *hcaA* gene locus, and the predicted *hcaA* gene locus after
568 homologous recombination are shown. (C, D) Confirmation of *hcaA* gene knockout. (C) PCR
569 using genomic DNA from wild-type (MRY08-1234 WT and MRY12-0027 WT) and HcaA-
570 knockout strains (MRY08-1234 Δ*hcaA* and MRY12-0027 Δ*hcaA*) as templates. Lane 1,
571 MRY12-0027 WT; Lane 2, MRY12-0027 *ΔhcaA*; Lane 3, MRY08-1234 WT; Lane 4, MRY08-
572 1234 *ΔhcaA*; Lane 5, OneSTEP Marker 6 (λ/Sty I digest) (Nippon Gene Co., Ltd.). White
573 arrows indicate amplicons of the *hcaA* gene (5,478 bp). Absence of the amplicons in HcaA-
574 knockout strains was confirmed. (D) Immunoblot of HcaA. The concentration of the extracted
575 protein was measured using the BCA protein assay. The samples were adjusted to a
576 concentration of 0.5 mg/mL with PBS and separated by 5–20% sodium dodecyl sulfate-
577 polyacrylamide gel electrophoresis. The top and bottom panels show results for MRY08-1234
578 and MRY12-0027, respectively. Lane M, Precision Plus Protein Dual Color Standards (Bio-
579 Rad); Lane 1 and 5, whole cell lysate; Lane 2 and 6, culture supernatant fraction; Lane 3 and 7,
580 membrane fraction; Lane 4 and 8, soluble fraction. The expected size of HcaA was 150 kDa,
581 and a band corresponding to 150 kDa was observed in the WT (lanes 1 and 3) but not in the
582 ΔHcaA strain (lanes 5 and 7), confirming the knockout and localization of HcaA.

583

584 Fig. 2. Knockout of HcaA reduced *H. cinaedi* cytotoxicity and adherence to cells.

585 (A) LDH assay to evaluate cytotoxicity. Each cell was infected with wild-type (MRY08-
586 1234 WT or MRY12-0027 WT) and HcaA-knockout (MRY08-1234 ΔHcaA or MRY12-0027
587 ΔHcaA) strains for 24 h (MOI 100). Cytotoxicity (%) was calculated using the method
588 described in the instructions. (B), (C), and (D): Adhesion and invasion assays against Caco-2
589 cells. Caco-2 cells were infected with wild-type (MRY08-1234 WT or MRY12-0027 WT) and
590 HcaA knockout (MRY08-1234 ΔHcaA or MRY12-0027 ΔHcaA) strains for 4 h (MOI 100).
591 The adhesion rate (B) and invasion rate (C) were calculated by dividing the number of adherent
592 bacterial cells and invading bacterial cells, respectively, by the total number of infected
593 bacterial cells. The invasion rate of adherent bacteria (D) was calculated by dividing the number
594 of invading bacteria cells by the number of adherent bacteria cells. Results are presented as the
595 mean ± standard deviation (SD) of six independent experiments. *, $P < 0.05$; **, $P < 0.01$; ***,
596 $P < 0.001$ ****, $P < 0.0001$; ns, not specified.
597
598 Fig. 3. RGD motif on HcaA contributes to the adhesion of *H. cinaedi*.
599 (A) SDS-PAGE of the purified WT HcaA and mutant HcaA, stained with Coomassie Brilliant
600 Blue (CBB). HcaA (120 kDa) with the RGD motif (WT HcaA) and HcaA with glycine replaced
601 with alanine in the RGD motif (Mutant HcaA) were expressed in *E. coli* and purified. Proteins
602 were adjusted to 1 mg/mL and applied. (B) Adhesion of purified WT HcaA (with the RGD
603 motif) and Mutant HcaA (with the RAD motif) to U937 cells. Fluorescence-labeled U937 cells
604 attached to HcaA were compared by measuring the fluorescence at 490 nm. Means and SD
605 reflect values of six per group. **, $P < 0.01$. (C) Three-dimensional structure of HcaA and HcaA
606 homologues predicted by AlphaFold2. Of the five models generated, the top-ranked model was
607 used in this study. The predicted structure was visualized using PyMOL Molecular Graphics
608 System Ver. 2.2.5. HcaA homologs from *H. bilis*, *H. fennelliae*, *H. canicola*, and *H. canis* were
609 analyzed and compared. The RGD motif is located at the protrusion in HcaA (within the square).

610 HcaA homologs had a structure protruding from the surface, like HcaA; however, the
611 protruding structure did not contain the RGD motif. (D) Phylogenetic tree based on the
612 alignment of the passenger domain of HcaA and HcaA homologs. The alignment was generated
613 using ClustalW ver. 2.1. The maximum-likelihood tree was constructed using RAxML
614 (https://github.com/amkozlov/raxml-ng) and visualized using MEGA-X v 10.2.6. A
615 comparison of the amino acid sequence of HcaA showed that the RGD motif was present only
616 in HcaA from *H. cinaedi* (red text).
617
618 Fig. 4. Knockout of HcaA reduced *H. cinaedi* colonization in mice.
619 (A) Anti-*H. cinaedi* antibody titers in infected mice, as determined by ELISA. Sera from
620 mice at 7, 14, and 28 days after inoculation were used. Squares and triangles indicate serum
621 from the group of infected wild-type (black square, MRY08-1234 WT; gray square, MRY12-
622 0027 WT) or HcaA knockout (black triangle, MRY08-1234 ΔHcaA; gray triangle, MRY12-
623 0027 ΔHcaA) strains, respectively. Means and SD reflect values from five of six mice per group.
624 **, $P < 0.01$. (B) Heatmap combining the results of the culture method and qPCR assays.
625 Columns indicate each mouse and rows indicate the duration of infection. Positive results for
626 both culture method and qPCR assays are shown in red, positive results for either are shown in
627 pink, and negative results for both are shown in light blue. (C) Quantitative bacteria count per
628 length of colon and representative images of the colon of *H. cinaedi*-infected mice. Adhesion
629 of *H. cinaedi* to the colon was quantified using ImageJ ver. 1.53t, by counting the number of *H.*
630 *cinaedi* in images taken with a 20× objective lens. Results are expressed as the number of *H.*
631 *cinaedi* per length of colon. Means and SD reflect the values of five or six mice per group. **,
632 $P < 0.01$. Green, *H. cinaedi*; blue, nucleus. Scale bar 100 um.

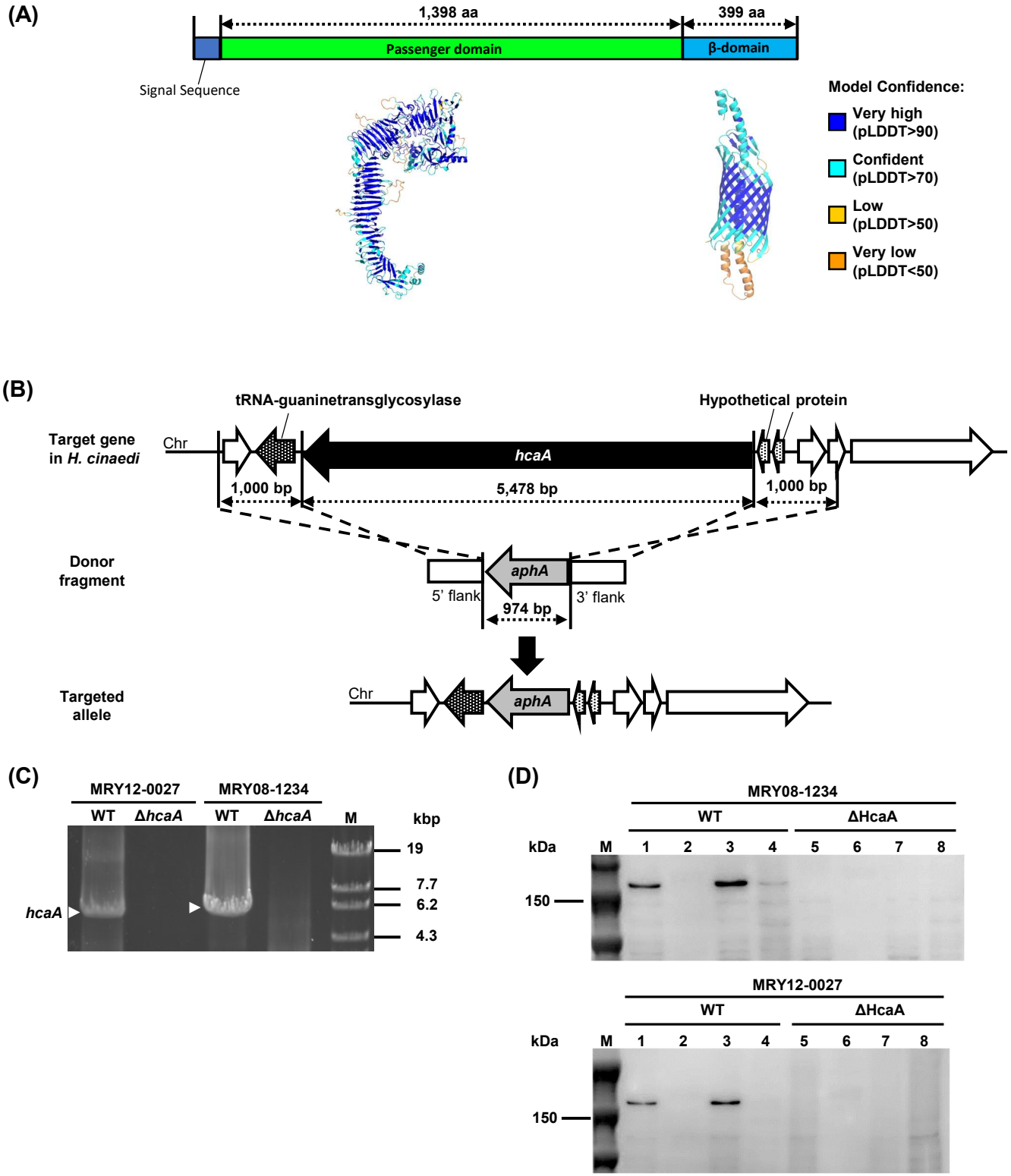
(A)
1,398 aa
399 aa
Passenger domain
β-domain
Signal Sequence
Model Confidence:
Very high (pLDDT>90)
Confident (pLDDT>70)
Low (pLDDT>50)
Very low (pLDDT<50)
(B)
tRNA-guaninetransglycosylase
Hypothetical protein
Target gene in H. cinaedi
Chr
hcaA
1,000 bp
5,478 bp
1,000 bp
Donor fragment
aphA
5' flank
3' flank
974 bp
Targeted allele
Chr
aphA
(C)
MRY12-0027
MRY08-1234
WT
ΔhcaA
WT
ΔhcaA
M
kbp
19
7.7
6.2
4.3
hcaA
(D)
MRY08-1234
WT
ΔHcaA
kDa
M
1
2
3
4
5
6
7
8
150
MRY12-0027
WT
ΔHcaA
kDa
M
1
2
3
4
5
6
7
8
150

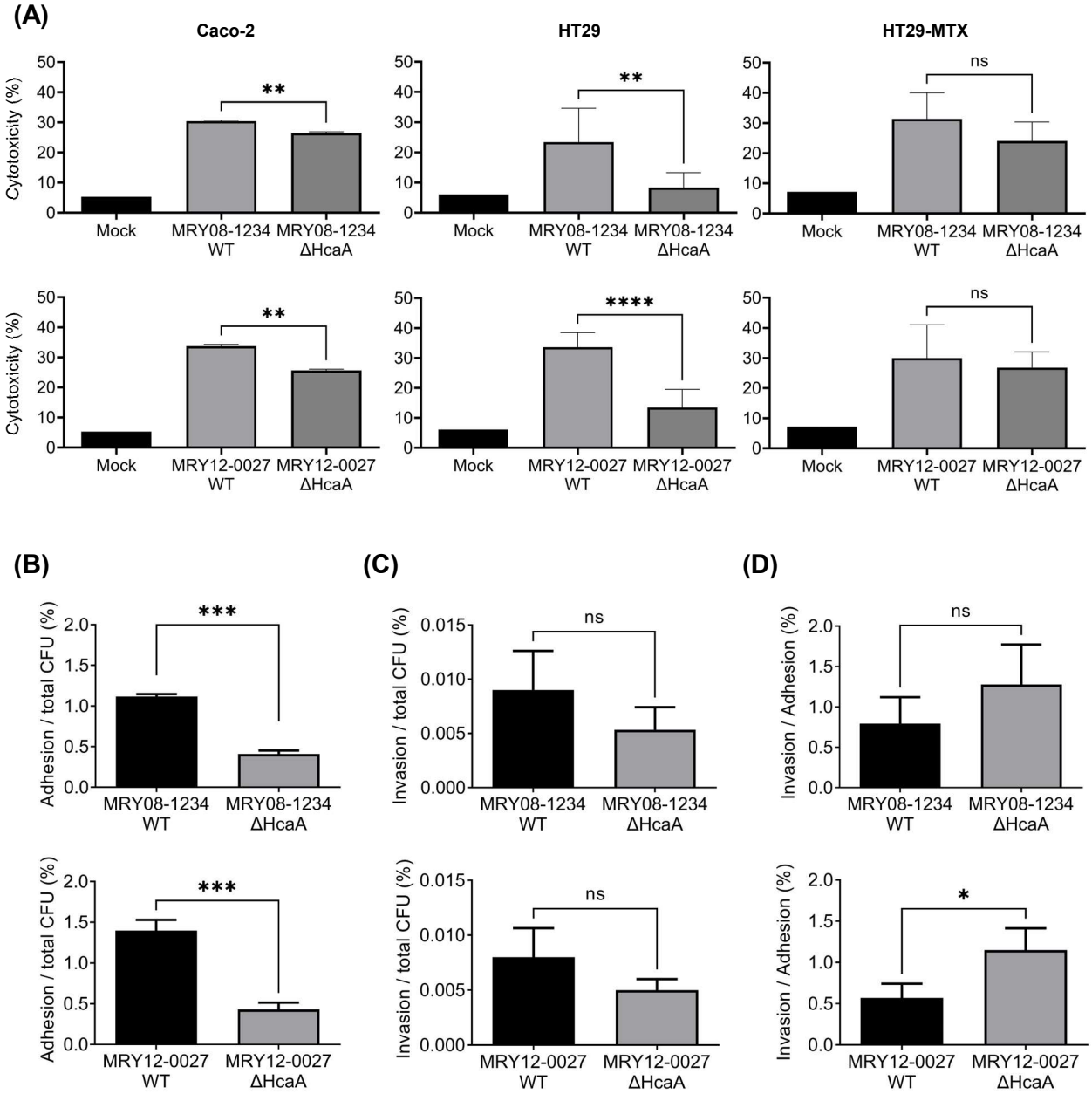
(A)
Caco-2
HT29
HT29-MTX
Cytotoxicity (%)
**
**
ns
**
****
ns
Mock
MRY08-1234 WT
MRY08-1234 ΔHcaA
MRY12-0027 WT
MRY12-0027 ΔHcaA
(B)
(C)
(D)
Adhesion / total CFU (%)
Invasion / total CFU (%)
Invasion / Adhesion (%)
***
ns
*

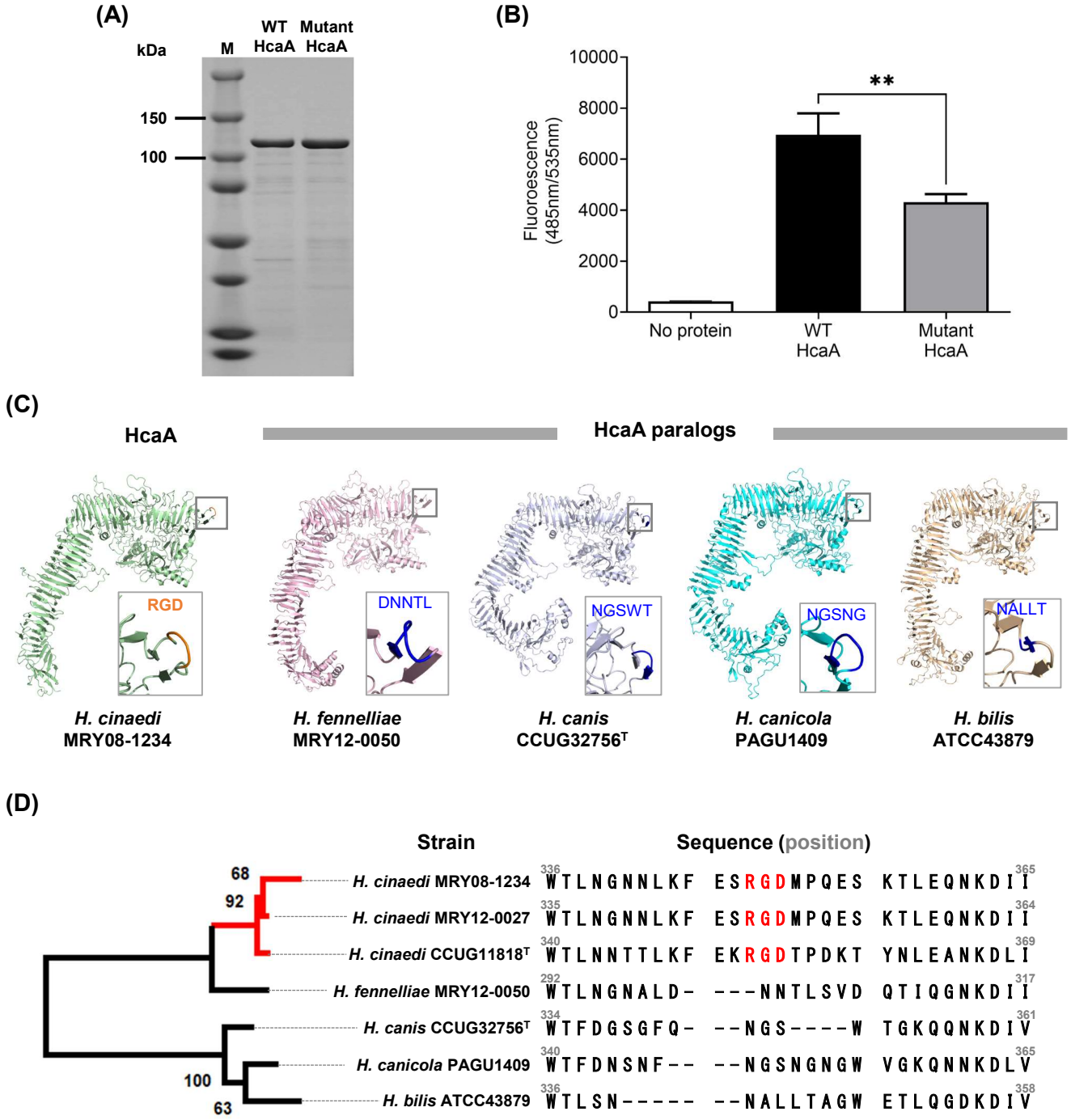
(A)
kDa
M
WT HcaA
Mutant HcaA
150
100
(B)
Fluoroescence (485nm/535nm)
10000
8000
6000
4000
2000
0
**
No protein
WT HcaA
Mutant HcaA
(C)
HcaA
HcaA paralogs
RGD
DNNTL
NGSWT
NGSNG
NALLT
H. cinaedi MRY08-1234
H. fennelliae MRY12-0050
H. canis CCUG32756T
H. canicola PAGU1409
H. bilis ATCC43879
(D)
Strain
Sequence (position)
68
92
100
63
H. cinaedi MRY08-1234 336 WTLNGNNLKF ESRGDMPQES KTLEQNKDII 365
H. cinaedi MRY12-0027 335 WTLNGNNLKF ESRGDMPQES KTLEQNKDII 364
H. cinaedi CCUG11818T 340 WTLNNTTLKF EKRGDTPDKT YNLEANKDLI 369
H. fennelliae MRY12-0050 292 WTLNGNALD- ---NNTLSVD QTIQGNKDII 317
H. canis CCUG32756T 334 WTFDGSGFQ- --NGS----W TGKQQNKDIV 361
H. canicola PAGU1409 340 WTFDNSNF-- --NGSNGNGW VGKQNNKDLV 365
H. bilis ATCC43879 336 WTLSN----- --NALLTAGW ETLQGDKDIV 358

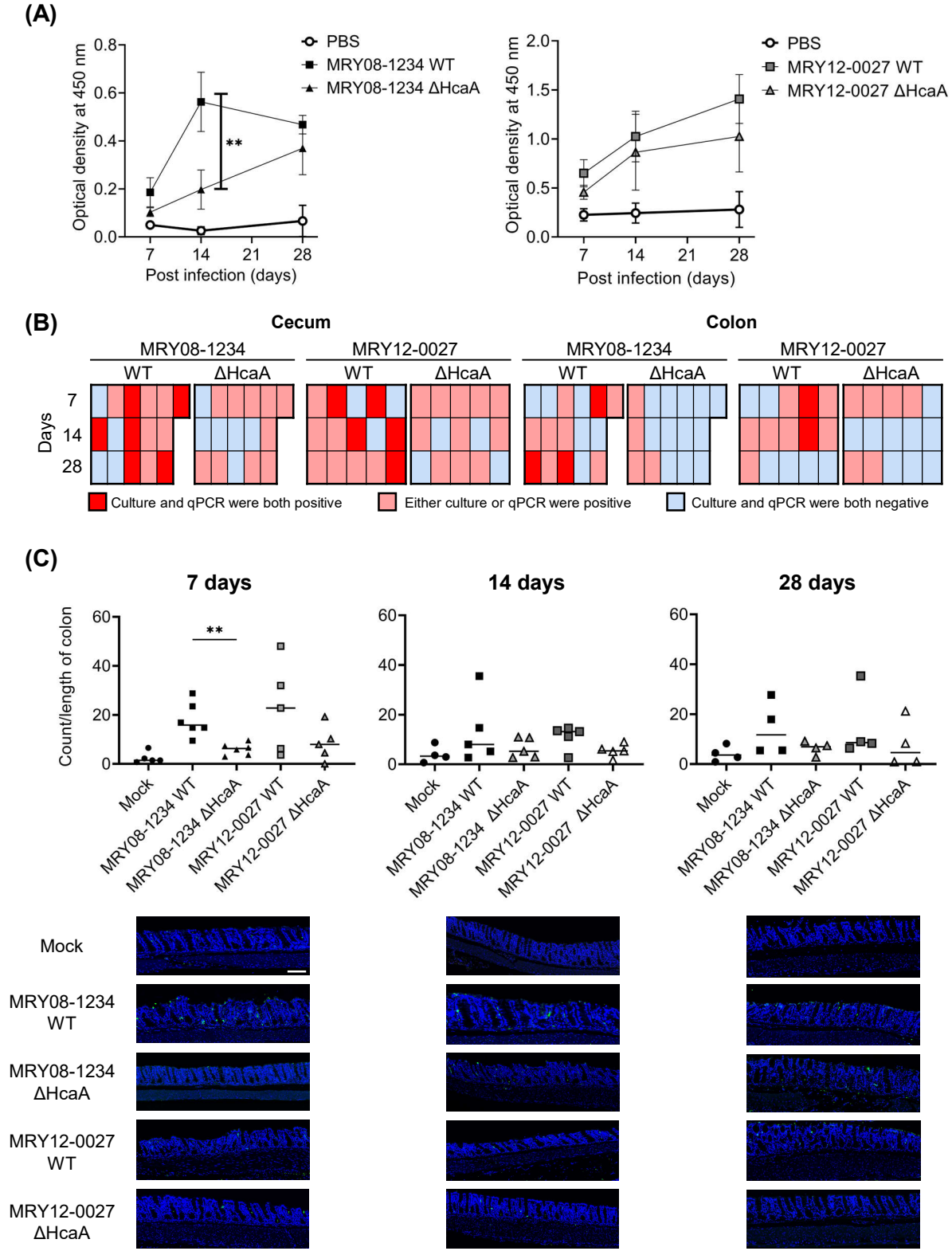
(A)
Optical density at 450 nm
Post infection (days)
PBS
MRY08-1234 WT
MRY08-1234 ΔHcaA
**
MRY12-0027 WT
MRY12-0027 ΔHcaA
(B)
Cecum
Colon
MRY08-1234
MRY12-0027
WT
ΔHcaA
Days
Culture and qPCR were both positive
Either culture or qPCR were positive
Culture and qPCR were both negative
(C)
7 days
14 days
28 days
Count/length of colon
Mock
MRY08-1234 WT
MRY08-1234 ΔHcaA
MRY12-0027 WT
MRY12-0027 ΔHcaA